ADVANCED QUANTUM TECHNOLOGIES
www.advquantumtech.com

Unusual Electrical and Magnetic Properties in Layered $EuZn_2As_2$

*Joanna Blawat, Madalynn Marshall, John Singleton, Erxi Feng, Huibo Cao, Weiwei Xie, and Rongying Jin**

Eu-based compounds often exhibit unusual magnetism, which is critical for nontrivial topological properties seen in materials such as $EuCd_2As_2$. The authors investigate the structure and physical properties of $EuZn_2As_2$ through measurements of the electrical resistivity, Hall effect, magnetization, and neutron diffraction. Their data show that $EuZn_2As_2$ orders antiferromagnetically with an A-type spin configuration below $T_N = 19$ K. Surprisingly, there is strong evidence for dominant ferromagnetic fluctuations above T_N, as reflected by positive Curie–Weiss temperature and extremely large negative magnetoresistance (MR) between T_N and $T_{fl} \approx 200$ K. Furthermore, the angle dependence of the MR_{ab} indicates field-induced spin reorientation from the *ab*-plane to a direction ≈45° from the *ab* plane. Compared to $EuCd_2As_2$, the doubled T_N and T_{fl} make $EuZn_2As_2$ a better platform for exploring nontrivial magnetic and electronic properties in both magnetic fluctuation ($T_N < T < T_{fl}$) and ordered ($T < T_N$) regimes.

1. Introduction

Since the discovery of topological states in semimetals,[1–6] the search for new topological materials has been extremely active. Time-reversal symmetry ($\mathcal{T}$) and crystal inversion symmetry ($\mathcal{P}$), together with the Kramers theorem (each energy band is doubly degenerate for fermions), are crucial in understanding the formation of topological states in semimetals.[1] When both $\mathcal{T}$ and $\mathcal{P}$ are preserved, a system may host Dirac fermions at the Dirac points (DP), at which bands are quadruply degenerate. Several Dirac semimetals have been identified, including Cd_3As_2,[2] Na_3Bi,[3] and $ZrTe_5$.[4] When $\mathcal{T}$ is broken but $\mathcal{P}$ is preserved, one may expect two Weyl cones with opposite chirality in a Weyl semimetal. Considering the opposite situation, that is, $\mathcal{T}$ is preserved but $\mathcal{P}$ is broken, the number of Weyl cones is a multiple of four, removing the chirality.[1] Weyl states have been observed in semimetals such as $MoTe_2$,[5,6] TaAs,[7] WTe_2,[8] and $TaIrTe_4$.[9] Breaking both $\mathcal{T}$ and $\mathcal{P}$ would generally destroy the Dirac/Weyl properties in these systems. An exception is that the Dirac state can exist if the symmetry of the product $\mathcal{PT}$ is preserved.[10] A case study was carried out in magnetic CuMnAs, which belongs to a type-III magnetic space group with a C-type spin structure.[11,12] Magnetic materials offer a fertile ground for searching for novel topological properties protected by the $\mathcal{PT}$ symmetry.

Recently, materials with the type-IV magnetic space group have also been studied.[13] The type-IV magnetic space group is defined by $G + \mathcal{T}\{e|\tau\}G$, where G is the ordinary nonmagnetic space group, e is the identity operation, and $\{e|\tau\}$ represents the translation operation between spin-up and spin-down sublattices in a magnetic space group.[13] In such a magnetic space group, there is a nonsymmorphic time-reversal $\mathcal{T}'$ symmetry, which is related to $\mathcal{T}$ through the translation operation τ ($\mathcal{T}' = \mathcal{T}\tau$). In the centrosymmetric type-IV magnetic space group, the symmetry of the product $\mathcal{PT}'$ is preserved; therefore Kramers degeneracy is protected, and Dirac points can exist.[13] $EuCd_2As_2$ has been theoretically predicted to be an antiferromagnetic (AFM) Dirac semimetal, in which DPs are protected by the $\mathcal{PT}'$ symmetry.[13] $EuCd_2As_2$ forms an A-type AFM state below $T_N = 9.5$ K in which the threefold symmetry in the *ab*-plane is broken due to the spin configuration. According to theoretical calculations, this leads to a gap between Dirac cones.[14,15] However, strong ferromagnetic

J. Blawat, R. Jin
Center for Experimental Nanoscale Physics
Department of Physics & Astronomy
University of South Carolina
Columbia, SC 29208, USA
E-mail: rjin@mailbox.sc.edu
J. Blawat
Department of Physics & Astronomy
Louisiana State University
Baton Rouge, LA 70803, USA
M. Marshall, W. Xie
Department of Chemistry and Chemical Biology
Rutgers University
Piscataway, NJ 08854, USA
J. Singleton
National High Magnetic Field Laboratory
Los Alamos National Laboratory
Los Alamos, NM 87545, USA
E. Feng, H. Cao
Neutron Scattering Division
Oak Ridge National Laboratory
Oak Ridge, TN 37831, USA
The ORCID identification number(s) for the author(s) of this article can be found under https://doi.org/10.1002/qute.202200012

DOI: 10.1002/qute.202200012

Table 1. Single crystal crystallographic data and structure refinement for $EuZn_2As_2$.

Formula	$EuZn_2As_2$
F. W. [g mol^{-1}]	432.54
Space group, Z	$P\text{-}3m1$ (#164)
a [Å]	4.2093(1)
b [Å]	4.2093(1)
c [Å]	7.175(3)
V [Å^3]	110.09(6)
Absorption correction	Numerical
Extinction coefficient	0.076(4)
Θ range [°]	2.839–33.143
hkl ranges	$-6 \le h \le 5$
	$-6 \le k \le 6$
	$-11 \le l \le 10$
No. reflections, R_{int}	1575, 0.0433
No. independent reflections	195
No. parameters	7
R_1, wR_2 [all I]	0.0258, 0.0378
Goodness of fit	1.084
Largest diff. peak and hole [e$^-$ Å^{-3}]	−1.477, 2.013

Table 2. Atomic coordinates and isotropic displacement parameters of $EuZn_2As_2$. U_{eq} is defined as one-third of the trace of the orthogonalized U_{ij} tensor (Å^2).

Atom	Wyckoff	Occupancy	x	y	z	U_{eq}
Eu	1b	1	0	0	0	0.0083(2)
Zn	2d	1	1/3	2/3	0.2667(9)	0.0074(2)
As	2d	1	1/3	2/3	0.6296(3)	0.0106(2)

(FM) fluctuations above T_N break the $\mathcal{T}$ symmetry, giving rise to a Weyl state at high temperatures ($T > T_N$).[16] The FM correlations in $EuCd_2As_2$ have been observed directly by resonant X-ray magnetic scattering.[17] Interestingly, only a single pair of Weyl nodes is found in the condition of field-induced full spin alignment along the c axis.[18] Thus, such a system provides a rare case for studying the transition between the Dirac and Weyl states by tuning temperature or field.

To further study the influence of magnetism on the topology of the electronic band structure, we investigate the physical properties of $EuZn_2As_2$, a sister compound of $EuCd_2As_2$. The replacement of Cd by Zn is expected to weaken the spin-orbit coupling, thus influencing the gap size between Dirac cones. In addition, compared to $EuCd_2As_2$, we find that the AFM ordering temperature for $EuZn_2As_2$, $T_N = 19$ K, is doubled, offering a much wider temperature range for studying potential topological properties in a long-range AFM ordered state. By analyzing magnetization and magneto-transport data, we also find strong evidence for FM fluctuations over a much wider temperature range than that in $EuCd_2As_2$. Such information is key toward the understanding of magnetism-driven topological properties of related compounds.

2. Results and Discussion

The single crystal X-ray diffraction refinement confirms that our crystals form a trigonal structure with the formula $EuZn_2As_2$. The space group is P-3m1 (No. 164) with the lattice parameters $a = b = 4.2093(1)$ Å and $c = 7.175(3)$ Å. Replacing Cd with smaller Zn, the lattice parameters in $EuZn_2As_2$ decrease more significantly along the a and b axes (≈5.5% reduction) than the c axis (≈2.4% reduction). Detailed information including atomic positions and sites occupancies is summarized in **Tables 1** and **2**. **Figure 1**a illustrates the crystal structure of $EuZn_2As_2$, where Zn (green) and As (grey) form a honeycomb network separated by Eu atoms (pink). Figure 1b shows the X-ray diffraction pattern of a flat surface of a $EuZn_2As_2$ single crystal at room temperature. All peaks can be indexed with the abovementioned structure from the (001) plane (i.e., the *ab*-plane). A weak peak near $2\Theta \approx 30°$ results from residual Sn on the surface. A picture of a $EuZn_2As_2$ single crystal is presented in the inset of Figure 1b. The powder X-ray diffraction (PXRD)pattern obtained from ground crystals was analyzed using the LeBail method and the result is presented in Figure S1, Supporting Information. The red points, black, and blue lines represent the experimentally observed intensities, calculated intensities, and the difference between them, respectively. The expected Bragg positions for $EuZn_2As_2$ are shown as green vertical marks. The LeBail analysis confirms that $EuZn_2As_2$ crystallizes in the abovementioned trigonal crystal structure.

Figure 2a shows the temperature dependence of the zero-field-cooled (ZFC) and field-cooled (FC) magnetic susceptibility ($\chi = M/H$) measured by applying a magnetic field of 0.1 T parallel to the c-axis (χ_c) and to the *ab*-plane (χ_{ab}), respectively. With decreasing temperature, both χ_{ab} and χ_c initially increase with little difference between them. Below $T_N = 19$ K, χ_{ab} tends to saturate but χ_c decreases. Such behavior suggests that the system forms an A-type AFM order, with FM alignment in the *ab*-plane but AFM coupling along the c-axis. The much higher T_N suggests stronger magnetic interactions both within the *ab* plane and along the c axis in $EuZn_2As_2$ than those in $EuCd_2As_2$,[19] consistent with the lattice parameter changes mentioned above.

To understand magnetic interactions in $EuZn_2As_2$, we fit χ_{ab} and χ_c between 100 and 300 K using the Curie–Weiss formula $\chi(T) = \chi_0 + C/(T-\theta)$, where χ_0 is a constant, θ is the Curie–Weiss temperature, and C is the Curie constant with $C = \frac{\mu_{eff}^2 N_A}{3k_B}$ (N_A is Avogadro constant and k_B is Boltzmann constant). As shown in the inset of Figure 2a, the formula fits the data well (the solid lines are fitting curves). The parameters obtained are $\chi_{0,ab} = -6.50 \times 10^{-3}$ cm^3 mol^{-1}, $\theta_{ab} = 15.1$ K, and $\mu^{ab}{}_{eff} = 8.42\mu_B$, and $\chi_{0,c} = -2.38 \times 10^{-3}$ cm^3 mol^{-1}, $\theta_c = 17.0$ K, and $\mu^{c}{}_{eff} = 8.26\mu_B$. The positive values of θ_{ab} and θ_c imply dominant FM interactions between Eu ions, with the effective magnetic moments close to the theoretical value for Eu^{2+} ($\mu_{eff} = g\sqrt{S(S+1)} \approx 3.97g$ with the Landé factor $g \approx 2$ if Eu^{2+} orbital moment is quenched). Furthermore, χ_{ab} measured under ZFC and FC modes shows no difference (Figure 2a). The application of higher magnetic field should enhance the FM interactions. Figure 2b,c shows the temperature dependences of χ_{ab} and χ_c between 2 and 60 K in various fields. Note that increased magnetic field pushes T_N to lower temperatures (Figure 2d). As shown in Figure 2e, the field dependence of

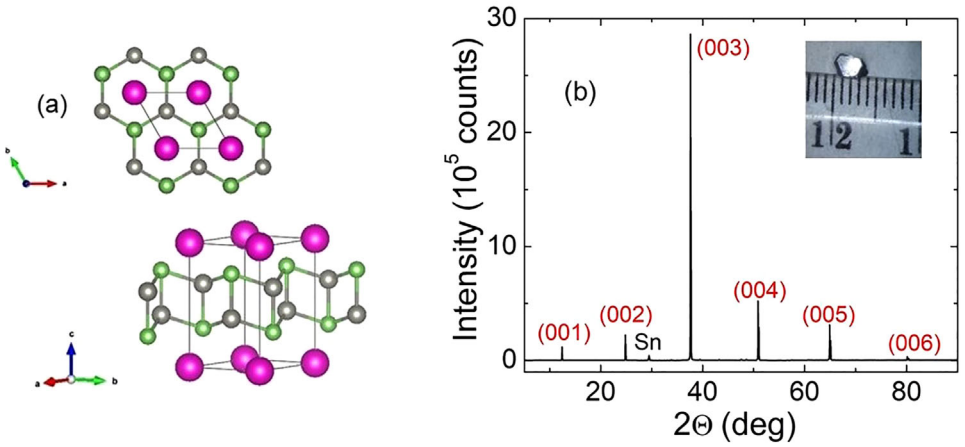

Figure 1. a) The crystal structure of $EuZn_2As_2$. The pink, green, and grey balls represent Eu, As, and Zn atoms, respectively. b) The XRD pattern of $EuZn_2As_2$ single crystal. Inset: picture of $EuZn_2As_2$ single crystal.

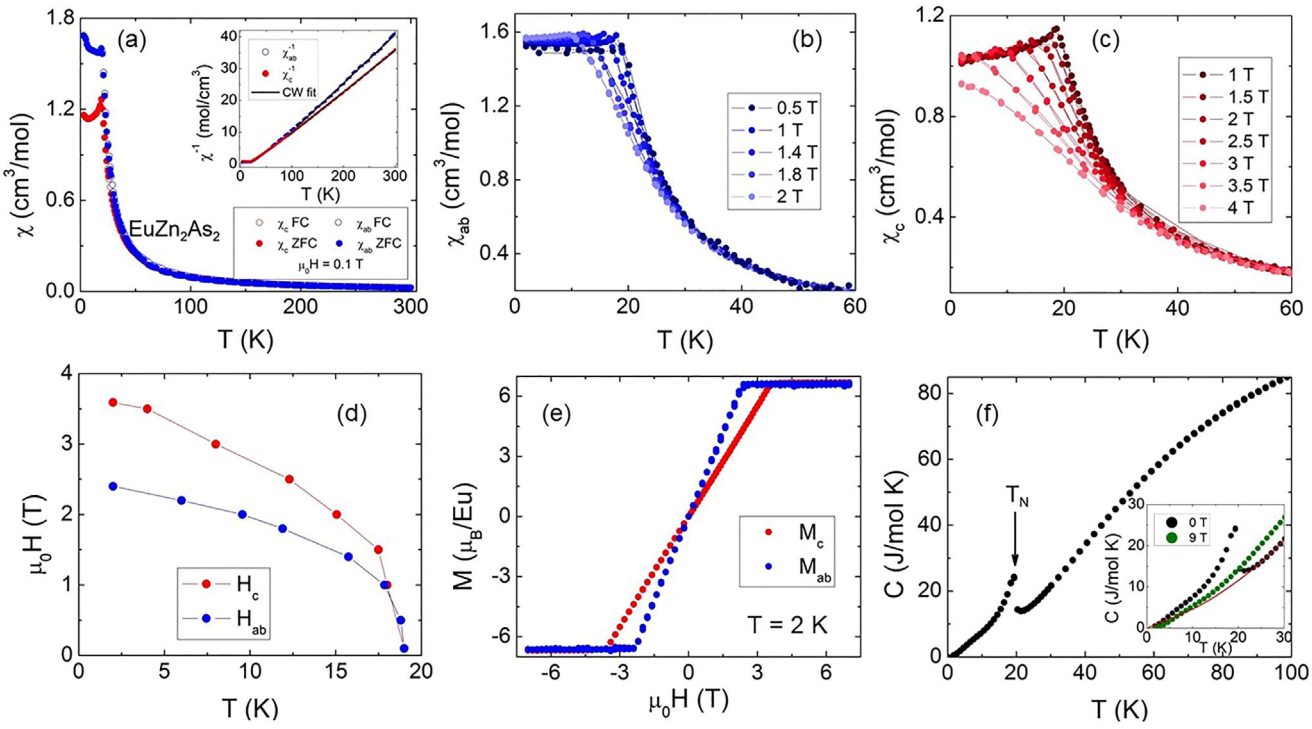

Figure 2. a) The temperature dependence of the magnetic susceptibility measured along *ab*-plane (χ_{ab}) and *c*-axis (χ_c). Inset: the inverse magnetic susceptibility measured along *ab*-plane and *c*-axis with the Curie–Weiss fit discussed in the text. b,c) χ_{ab} and χ_c measured at several magnetic fields as a function of temperature, respectively. d) H–T phase diagram constructed using χ_{ab} and χ_c in (b) and (c). e) Magnetic hysteresis loop measured along the *ab*-plane (M_{ab}) and *c*-axis (M_c) at $T = 2$ K. f) The temperature dependence of specific heat. Inset: the specific heat measured with $H = 0$ and 9 T. The solid line represents the background specific heat consisting of contributions from electrons and phonons at $H = 0$.

the magnetization has no hysteresis in either M_{ab} or M_c at 2 K. Instead, both M_{ab}(H) and M_c(H) vary linearly with field before reaching saturation. The observed saturation moment is close to the theoretical value for Eu^{2+} ($\mu_{sat} = gJ = 7\mu_B$, where J is the total angular momentum).[20]

To confirm the nature of the phase transition at T_N, we have measured the temperature and field dependence of the specific heat, C_p. Figure 2f shows the temperature dependence of C_p at $\mu_0 H = 0$ and 9 T. Note that there is a lambda-shaped anomaly in $C_p(H = 0)$ at $T_N = 19$ K, indicating a second-order phase transition. To estimate the entropy associated with the phase transition, we subtract the electronic and phonon specific heat by fitting data between 1.8 and 4 K and between 25 and 30 K using $C_p = \gamma T + \beta T^3$ (γ and β are constants), as plotted in the inset of Figure 2f. The entropy change $\Delta S \approx 11.2$ J mol^{-1} K^{-1}, about 65% of the theoretically expected value for an eightfold

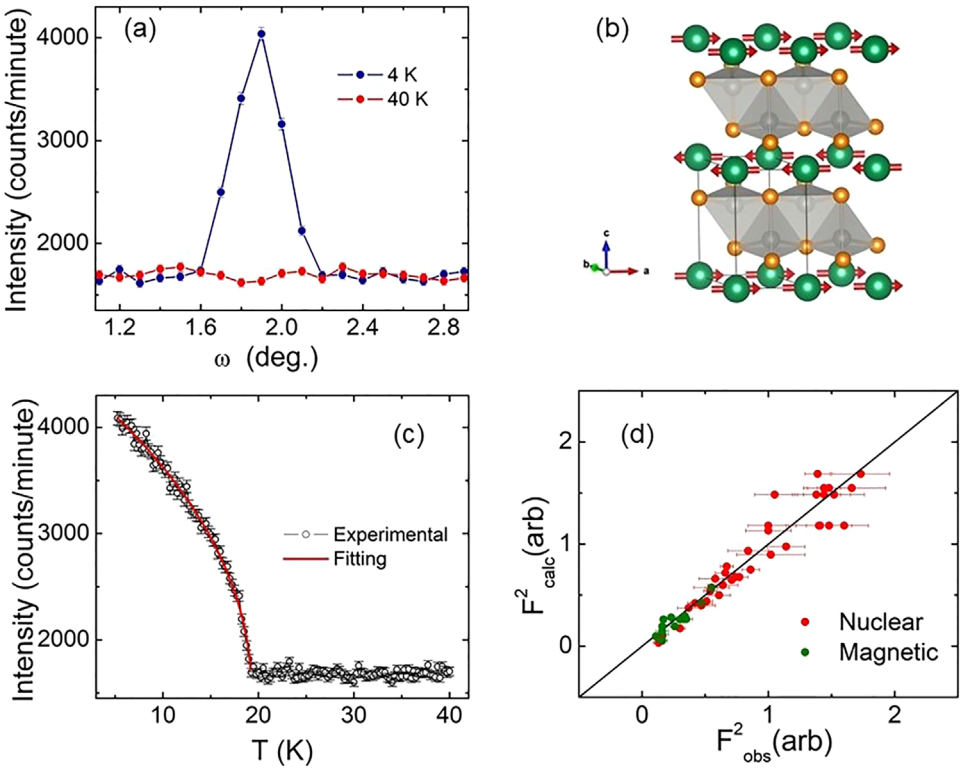

Figure 3. a) The rocking curve scans at (0 0 ½) at 4 and 40 K, measured by neutrons. b) Magnetic structure of Eu sublattice obtained at $T = 4$ K. c) The peak intensity as a function of temperature with the empirical law fit (red solid line) discussed in the text. d) Calculated structure factor square (F^2_{calc}) versus the observed one (F^2_{obs}).

degenerate system ($\Delta S = R\ln(2J+1) = R\ln 8 = 17.28$ J mol^{-1} K^{-1}). This reduced entropy is likely related to magnetic fluctuations, which release some amount of entropy above T_N. By applying $\mu_0 H = 9$ T, the specific heat peak is completely suppressed. Notably, C_p ($\mu_0 H = 9$ T) > C_p ($H = 0$) above 19 K, suggesting that the magnetic entropy associated with the transition is distributed through a larger temperature range above T_N.

Given the unusual magnetic behavior seen in the magnetization above and below T_N, it is essential to determine the magnetic structure of $EuZn_2As_2$ through single-crystal neutron diffraction experiment. **Figure 3**a shows the rocking curve scan at (0 0 ½) peak position at 4 and 40 K. The peak disappears above T_N, indicating a magnetic propagation vector k = (0 0 ½) for the ordered state. We find that the magnetic peaks collected at 4 K can be fit by an A-type magnetic structure with the magnetic moments entirely in the *ab*-plane within the data resolution. The resultant magnetic structure at 4 K is presented in Figure 3b, which is ferromagnetically aligned in the *ab* plane but AFM along the *c* axis. This A-type AFM structure is the same as those seen in $EuCd_2As_2$ grown with Sn flux,[15,19] $EuCd_2Sb_2$,[21] and in $EuMg_2Bi_2$[22] but different from that in $EuIn_2As_2$.[23] At 4 K, the refined magnetic moment is $7.33(7)\mu_B$/Eu, slightly higher than the saturation value from the magnetization (Figure 2e). We choose the reflection intensity (I) at (0 0 ½) as the order parameter. The temperature dependence of I is shown in Figure 3c. The solid curve is the fit of $I(T)$ to $I = A(1 - T/T_N)^{2\beta} + B$, with $T_N \approx 19.4$ K, $A = 3119$, $\beta = 0.23$, and $B = 1394$. The critical exponent β obtained corresponds to a 2D magnetic system, consistent with the layered structure of $EuZn_2As_2$. Figure 3d shows the calculated structure factor square (F^2_{calc}) versus the observed one (F^2_{obs}). The linear behavior indicates excellent structure refinement. Any deviation is likely to be due to the errors resulting from the absorption correction process.

With an A-type magnetic structure (Figure 3b), it is necessary to ask why θ_c, obtained at temperatures well above T_N, is positive. For $EuCd_2As_2$, both electron-spin resonance and muon-spin relaxation measurements reveal strong FM fluctuations with long time and length scales, which persist up to ≈100 K.[16] Although this was not discussed in ref. [16], we note that the electrical resistivity of $EuCd_2As_2$ also begins to show a negative slope below around 100 K. Bearing this in mind, we investigate the temperature and field dependence of both the *ab*-plane (ρ_{ab}, $I \parallel ab$) and *c*-axis (ρ_c, $I \parallel c$) resistivities. **Figure 4**a shows the temperature dependence of ρ_{ab} and ρ_c between 2 and 300 K for $EuZn_2As_2$. Several features are worth mentioning. First, while $\rho_c > \rho_{ab}$ due to the layered structure of $EuZn_2As_2$, ρ_{ab} and ρ_c show similar temperature dependence over the entire temperature range. This implies that the scattering mechanism is more or less the same in both the *ab* plane and the *c* direction. Similar behavior has also been reported for $EuCd_2As_2$.[24] Second, there is a sharp peak in both ρ_{ab} and ρ_c, corresponding to the magnetic transition at T_N. The peak in ρ_c is even sharper than that in ρ_{ab}. Third, both ρ_{ab} and ρ_c initially vary linearly with temperature at high temperatures, deviating below $T_{fl} \approx 200$ K and eventually acquiring negative slopes ($d\rho_{ab}/dT < 0$ and $d\rho_c/dT < 0$) below ≈150 K. The sharp

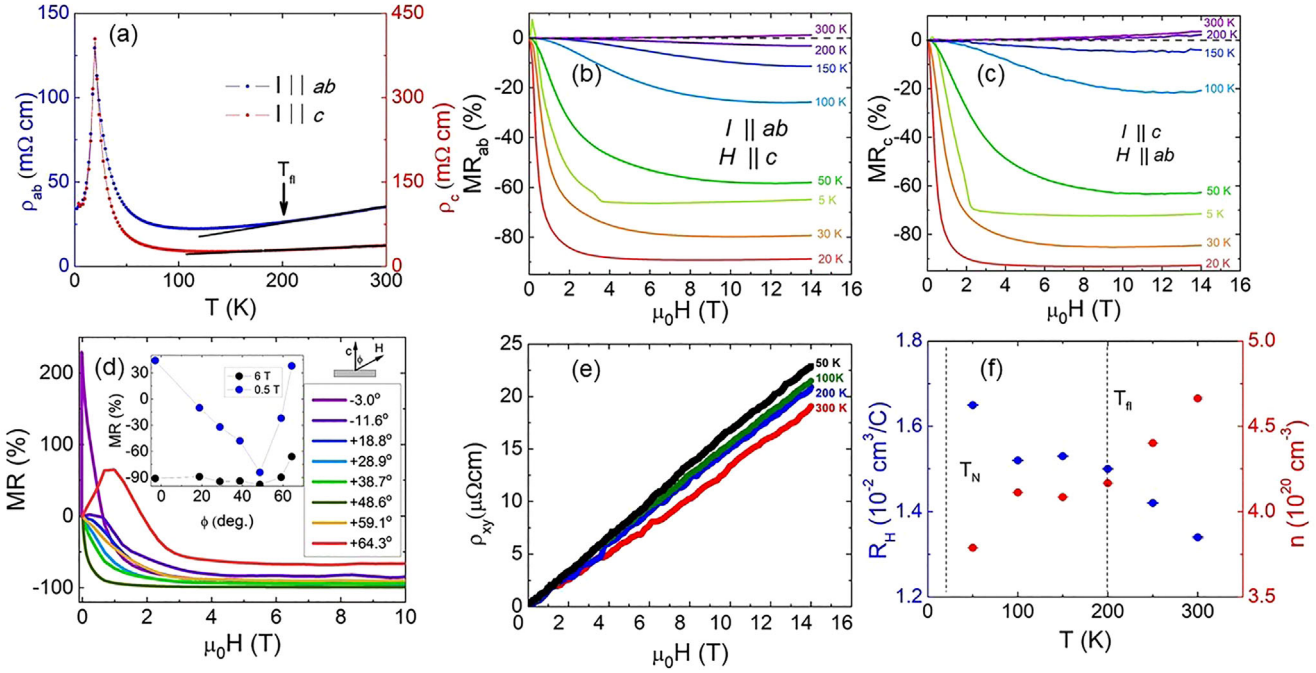

Figure 4. a) Electrical resistivity as a function of temperature measured along *ab*-plane and *c*-axis. b) MR_{ab} and c) MR_c measured at several temperatures. d) Magnetic field dependence of magnetoresistivity measured at several different angles. Inset: magnetoresistivity versus angle taken at magnetic field $\mu_0 H = 0.5$ and 6 T. e) Magnetic field dependence of the Hall effect. f) Hall coefficient and charge density as a function of temperature.

decrease of ρ_{ab} and ρ_c below T_N indicates that the resistivity in all directions is dominated by spin scattering above T_N. The departure from the high-temperature linear behavior marks the spin scattering contribution to the resistivity due to magnetic fluctuations below T_{fl}.

To confirm the effect of magnetic fluctuations on ρ_{ab} and ρ_c, the magnetic field dependence of ρ_{ab} and ρ_c at constant temperatures is investigated. Figure 4b,c shows the field dependence of the transverse ($H \perp I$) magnetoresistivity MR_{ab} ($I \parallel ab$, $H \parallel$ c) and MR_c ($I \parallel$ c, $H \parallel ab$) at various temperatures between 2 and 300 K, respectively. MR is defined by $MR = \frac{\rho(H)-\rho(H=0)}{\rho(H=0)} \times 100\%$. At 300 K, both MR_{ab} and MR_c are small and positive, typical for a paramagnetic material. Quantitatively, both MR_{ab} (300 K) and MR_c (300 K) follow the H^2 behavior as expected. Upon cooling, both MR_{ab} and MR_c gradually decrease and become negative near 200 K. The field dependence of both MR_{ab} and MR_c also deviates from the H^2 behavior. With further cooling, their magnitudes continuously increase until T_N. The negative MR_{ab} and MR_c indicate the influence of FM fluctuation below $T_{fl} \approx 200$ K, consistent with what is seen in $EuCd_2As_2$.[16] Note that T_{fl} for $EuZn_2As_2$ is much higher than that in $EuCd_2As_2$. Both higher T_{fl} and T_N offer wider temperature ranges for studying magnetism-related properties in $EuZn_2As_2$ than in $EuCd_2As_2$.

At T_N, the spin scattering is almost completely suppressed by the application of the magnetic field, so that MR_{ab} and MR_c reach $\approx -90\%$ at $H > H_{sat}$. Below T_N, the field dependence of both MR_{ab} and MR_c is nonmonotonic, with an initial increase followed by a decrease to negative values (Figure 4b,c). The initial positive MR_c is attributable to AFM interaction in the *c* direction (Figure 3a).[25] Positive MR_{ab} should be related to the change in population of magnetic domains with the applied field. With increasing field (less than 1 Tesla at 5 K), both MR_{ab} and MR_c start to decrease, eventually becoming negative and saturated above H_{sat}. This implies continuous alignment toward the FM configuration. When H reaches H_{sat}, all moments are aligned ferromagnetically. Figure 4d shows the field dependence of MR_{ab} at various angles ϕ ($\phi = H \hat{} I$ – defined in the inset, changing from transverse [0°] to longitudinal [90°]) at $T = 0.6$ K. The low-field MR_{ab} peak is gradually suppressed as H turns away from the principal axes (*ab*- or *c*-axis). The inset of Figure 4d shows $MR_{ab}(\phi)$ at $\mu_0 H = 0.5$ and 6 T. Note that $MR_{ab}(\phi)$ reaches a minimum around $\phi = 45°$, implying that there is field-induced spin reorientation. The preferable field-induced spin direction is 45° between the *ab*-plane and *c*-axis, resulting in least spin scattering. This indicates that the magnetic configuration is extremely susceptible to the magnetic field.

With a strong magnetic fluctuation effect on the resistivity observed, it is interesting to consider the Hall response. Figure 4e shows the magnetic field dependence of the Hall resistivity (ρ_{xy}) at temperatures between T_N and 300 K. Note that ρ_{xy} increases linearly with the magnetic field at high temperatures, but deviation occurs when approaching T_N. For each temperature, we fit data between 0 and 14 T to $\rho_{xy} = \mu_0 R_H H$, where R_H is a Hall coefficient. Figure 4f presents the temperature dependence of R_H, which increases with decreasing temperature. The positive R_H suggests that holes are dominant carriers in $EuZn_2As_2$. Using the Drude relationship for a single band case with $R_H = -1/ne$, the carrier concentration n can be estimated. As shown in Figure 4f, $n \approx 4.6 \times 10^{20}$ cm^{-3} at room temperature, consistent with the semimetallic scenario for $EuZn_2As_2$. It increases slightly with

increasing temperature, which can be attributed to thermal effect if there is a small band gap as predicted in $EuCd_2As_2$. It is our future work to elucidate the connection between magnetic fluctuations and possible topological phase transition in $EuZn_2As_2$ as discussed in $EuCd_2As_2$.[14–16]

3. Summary

We have successfully grown single crystalline $EuZn_2As_2$, which forms a trigonal structure. The electrical resistivity, magnetization, and neutron diffraction investigation indicate that $EuZn_2As_2$ orders antiferromagnetically below $T_N = 19$ K with an A-type spin configuration. Similar to $EuCd_2As_2$, there are strong FM fluctuations that give rise to profound spin scattering between T_N and $T_{fl} \approx 200$ K in $EuZn_2As_2$. Our MR_{ab} measurements with variable applied field direction indicate that there is field-induced reorientation of the spins to ≈45° between the *ab*-plane and *c*-axis. Compared to $EuCd_2As_2$, the doubled T_N and T_{fl} make $EuZn_2As_2$ a better platform for exploring topological properties in both magnetic fluctuation ($T_N < T < T_{fl}$) and ordered ($T < T_N$) regimes. It is especially interesting to find out 1) if the reduced spin-orbit coupling in $EuZn_2As_2$ will reduce or close the gap between Dirac cones predicted in $EuCd_2As_2$, 2) if the canted spin structure induced by magnetic field impacts the topological states, and 3) where the Dirac/Weyl points in $EuZn_2As_2$ are located relative to the Fermi energy, and whether or not nontrivial electronic bands cross the Fermi level.

4. Experimental Section

The single crystals of $EuZn_2As_2$ were grown via the flux method using Sn. The elemental Eu (99.9% pieces, Alfa Aesar), Zn (99.8% granules, Alfa Aesar), As (99.999% powder, Alfa Aesar), and Sn (99.9% granules, Alfa Aesar) were placed into an alumina crucible with a molar ratio Eu:Zn:As:Sn = 1:2:2:20, and sealed in an evacuated quartz tube. The sample was heated up to 600 °C at a rate of 60 °C h^{-1}, and kept at this temperature for 5 h. This was followed warming to 1000 °C and tempering for 10 h. The sample was then slowly cooled (−3 °C h^{-1}) down to 600 °C with a further centrifuge in order to remove Sn flux. The resulting single crystals had a typical size of 4 mm × 2 mm × 1 mm and were stable in air.

The crystal structure was determined by single crystal X-ray diffraction using a Bruker Apex II single X-ray diffractometer equipped with Mo radiation ($\lambda_{K\alpha} = 0.71073$ Å), and by PXRD by means of a Rigaku MiniFlex 600 diffractometer with Cu $K_{\alpha 1}$ radiation ($\lambda = 1.5406$ Å). The crystal structure was solved with the full-matrix least-squares method using the SHELXTL package.[26] The PXRD pattern was analyzed using the FullProf software.[10] The crystal structure was drawn by means of VESTA software.[27]

The magnetic properties were measured in a Quantum Design Magnetic Properties Measurement System (7 T). The electrical resistivity, Hall effect, and heat capacity were measured using a Quantum Design Physical Property Measurement System (14 T). The standard four-probe technique was used to measure the electrical resistivity and Hall effect, and the relaxation method was used for the heat capacity. For both the electrical resistivity and Hall effect measurements, four thin Pt wires were attached to a sample using silver epoxy. The contact resistance was 10–50 Ω. To eliminate signal from possible contact misalignment, both magnetoresistance (MR) and Hall resistivity (ρ_{xy}) were obtained by sweeping the magnetic field between −14 and +14 T, that is, MR = [MR(+H)+MR(-H)]/2 and $\rho_{xy} = [\rho_{xy}(+H) - \rho_{xy}(-H)]/2$. The angle dependence of the MR was measured at the pulsed-field facility of National High Magnetic Field Laboratory (NHMFL, Los Alamos).

To determine the magnetic structure of $EuZn_2As_2$, single-crystal neutron diffraction experiment was performed on DEMAND (HB-3A) at the High Flux Isotope Reactor of Oak Ridge National Laboratory.[28] A wavelength of 1.008 Å from the bent Si-331 monochromator was used to reduce the heavy neutron absorption. Considering the large neutron absorption coefficient of Eu, PLATON software was employed to apply an absorption correction.[29,30] The magnetic and nuclear structures were both determined using Fullprof refinement Suite software.[10]

Supporting Information

Supporting Information is available from the Wiley Online Library or from the author.

Acknowledgements

Work at University of South Carolina and Louisiana State University was supported by NSF through Grant DMR-1504226. M.M. and W.X. were supported by the U.S. Department of Energy (DOE), Office of Science, Basic Energy Sciences under award DE-SC0022156. E.F. and H.B.C. were supported by the U.S. DOE, Office of Science, Office of Basic Energy Sciences, Early Career Research Program Award KC0402020, under Contract No. DE-AC05-e00OR22725. This research used resources at the High Flux Isotope Reactor and the Spallation Neutron Source, the DOE Office of Science User Facility operated by ORNL. A portion of this work was performed at the National High Magnetic Field Laboratory (NHMFL), which was supported by National Science Foundation Cooperative Agreement No. DMR-1644779 and the Department of Energy (DOE). J.S. acknowledges support from the DOE BES program "Science at 100 T," which permitted the design and construction of specialized equipment used in the high-field studies.

Conflict of Interest

The authors declare no conflict of interest.

Data Availability Statement

The data that support the findings of this study are available from the corresponding author upon reasonable request.

Keywords

antiferromagnetic orders, ferromagnetic fluctuations, topological states, type-IV magnetic space group

Received: February 8, 2022
Revised: March 24, 2022
Published online:

[1] M. Z. Hasan, C. L. Kane, *Rev. Mod. Phys.* **2010**, *82*, 3045.
[2] Z. K. Liu, J. Jiang, B. Zhou, Z. J. Wang, Y. Zhang, H. M. Weng, D. Prabhakaran, S.-K. Mo, H. Peng, P. Dudin, T. Kim, M. Hoesch, Z. Fang, X. Dai, Z. X. Shen, D. L. Feng, Z. Hussain, Y. L. Chen, *Nat. Mater.* **2014**, *13*, 677.
[3] Z. K. Liu, B. Zhou, Y. Zhang, Z. J. Wang, H. M. Weng, D. Prabhakaran, S.-K. Mo, Z. X. Shen, Z. Fang, X. Dai, Z. Hussain, Y. L. Chen, *Science* **2014**, *343*, 864.
[4] G. Zheng, J. Lu, X. Zhu, W. Ning, Y. Han, H. Zhang, J. Zhang, C. Xi, J. Yang, H. Du, K. Yang, Y. Zhang, M. Tian, *Phys. Rev. B* **2016**, *93*, 115416.

[5] J. Jiang, Z. K. Liu, Y. Sun, H. F. Yang, C. R. Rajamathi, Y. P. Qi, L. X. Yang, C. Chen, H. Peng, C.-C. Hwang, S. Z. Sun, S.-K. Mo, I. Vobornik, J. Fujii, S. S. P. Parkin, C. Felser, B. H. Yan, Y. L. Chen, *Nat. Commun.* **2017**, *8*, 13973.
[6] K. Deng, G. Wan, P. Deng, K. Zhang, S. Ding, E. Wang, M. Yan, H. Huang, H. Zhang, Z. Xu, J. Denlinger, A. Fedorov, H. Yang, W. Duan, H. Yao, Y. Wu, S. Fan, H. Zhang, X. Chen, S. Zhou, *Nat. Phys.* **2016**, *12*, 1105.
[7] B. Q. Lv, H. M. Weng, B. B. Fu, X. P. Wang, H. Miao, J. Ma, P. Richard, X. C. Huang, L. X. Zhao, G. F. Chen, Z. Fang, X. Dai, T. Qian, H. Ding, *Phys. Rev. X* **2015**, *5*, 031013.
[8] P. Li, Y. Wen, X. He, Q. Zhang, C. Xia, Z.-M. Yu, S. A. Yang, Z. Zhu, H. N. Alshareef, X.-X. Zhang, *Nat. Commun.* **2017**, *8*, 2150.
[9] I. Belopolski, P. Yu, D. S. Sanchez, Y. Ishida, T.-R. Chang, S. S. Zhang, S.-Y. Xu, H. Zheng, G. Chang, G. Bian, H.-T. Jeng, T. Kondo, H. Lin, Z. Liu, S. Shin, M. Z. Hasan, *Nat. Commun.* **2017**, *8*, 942.
[10] J. Rodríguez-Carvajal, *Phys. B* **1993**, *192*, 55.
[11] E. Emmanouilidou, H. Cao, P. Tang, X. Gui, C. Hu, B. Shen, J. Wu, S.-C. Zhang, W. Xie, N. Ni, *Phys. Rev. B* **2017**, *96*, 224405.
[12] S.-G. Xu, Z.-J. Chen, X.-B. Chen, Y.-J. Zhao, H. Xu, X. Zhang, *Phys. Rev. B* **2020**, *102*, 125123.
[13] G. Hua, S. Nie, Z. Song, R. Yu, G. Xu, K. Yao, *Phys. Rev. B* **2018**, *98*, 201116.
[14] J. Ma, H. Wang, S. Nie, C. Yi, Y. Xu, H. Li, J. Jandke, W. Wulfhekel, Y. Huang, D. West, P. Richard, A. Chikina, V. N. Strocov, J. Mesot, H. Weng, S. Zhang, Y. Shi, T. Qian, M. Shi, H. Ding, *Adv. Mater.* **2020**, *32*, 1907565.
[15] M. C. Rahn, J.-R. Soh, S. Francoual, L. S. I. Veiga, J. Strempfer, J. Mardegan, D. Y. Yan, Y. F. Guo, Y. G. Shi, A. T. Boothroyd, *Phys. Rev. B* **2018**, *97*, 214422.
[16] J.-Z. Ma, S. M. Nie, C. J. Yi, J. Jandke, T. Shang, M. Y. Yao, M. Naamneh, L. Q. Yan, Y. Sun, A. Chikina, V. N. Strocov, M. Medarde, M. Song, Y.-M. Xiong, G. Xu, W. Wulfhekel, J. Mesot, M. Reticcioli, C. Franchini, C. Mudry, M. Müller, Y. G. Shi, T. Qian, H. Ding, M. Shi, *Sci. Adv.* **2019**, *5*, eaaw4718.
[17] J.-R. Soh, E. Schierle, D. Y. Yan, H. Su, D. Prabhakaran, E. Weschke, Y. F. Guo, Y. G. Shi, A. T. Boothroyd, *Phys. Rev. B* **2020**, *102*, 014408.
[18] J.-R. Soh, F. de Juan, M. G. Vergniory, N. B. M. Schröter, M. C. Rahn, D. Y. Yan, J. Jiang, M. Bristow, P. Reiss, J. N. Blandy, Y. F. Guo, Y. G. Shi, T. K. Kim, A. McCollam, S. H. Simon, Y. Chen, A. I. Coldea, A. T. Boothroyd, *Phys. Rev. B* **2019**, *100*, 201102.
[19] N. H. Jo, B. Kuthanazhi, Y. Wu, E. Timmons, T.-H. Kim, L. Zhou, L.-L. Wang, B. G. Ueland, A. Palasyuk, D. H. Ryan, R. J. McQueeney, K. Lee, B. Schrunk, A. A. Burkov, R. Prozorov, S. L. Bud'ko, A. Kaminski, P. C. Canfield, *Phys. Rev. B* **2020**, *101*, 140402.
[20] J. Jensen, A. R. Mackintosh, *Rare Earth Magnetism*, Clarendon Press, Oxford **1991**.
[21] J.-R. Soh, C. Donnerer, K. M. Hughes, E. Schierle, E. Weschke, D. Prabhakaran, A. T. Boothroyd, *Phys. Rev. B* **2018**, *98*, 064419.
[22] S. Pakhira, T. Heitmann, S. X. M. Riberolles, B. G. Ueland, R. J. McQueeney, D. C. Johnston, D. Vaknin, *arXiv:2009.06880* **2020**.
[23] S. X. M. Riberolles, T. V. Trevisan, B. Kuthanazhi, T. W. Heitmann, F. Ye, D. C. Johnston, S. L. Bud'ko, D. H. Ryan, P. C. Canfield, A. Kreyssig, A. Vishwanath, R. J. McQueeney, L.-L. Wang, P. P. Orth, B. G. Ueland, *Nat. Commun.* **2021**, *12*, 999.
[24] H. P. Wang, D. S. Wu, Y. G. Shi, N. L. Wang, *Phys. Rev. B* **2016**, *94*, 045112.
[25] H. Yamada, S. Takada, *J. Phys. Soc. Jpn.* **1973**, *34*, 51.
[26] G. M. Sheldrick, *Acta Crystallogr., Sect. C: Struct. Chem.* **2015**, *71*, 3.
[27] K. Momma, F. Izumi, *J. Appl. Crystallogr.* **2011**, *44*, 1272.
[28] H. Cao, B. C. Chakoumakos, K. M. Andrews, Y. Wu, R. A. Riedel, J. Hodges, W. Zhou, R. Gregory, B. Haberl, J. Molaison, G. W. Lynn, *Crystals* **2019**, *9*, 5.
[29] A. L. Spek, *J. Appl. Crystallogr.* **2003**, *36*, 7.
[30] A. L. Spek, *Acta Crystallogr., Sect. C: Struct. Chem.* **2015**, *71*, 9.